Multiple Dot-in-Rod PbS/CdS Heterostructures with High Photoluminescence Quantum Yield in the Near-Infrared

Yolanda Justo,[†,‡] Bart Goris,[⊥] John Sundar Kamal,[†,‡] Pieter Geiregat,[†,‡,§] Sara Bals,[⊥] and Zeger Hens*[,†,‡]

[†]Physics and Chemistry of Nanostructures, [‡]Center for Nano and Biophotonics, and [§]Photonics Research Group, Ghent University, B-9000 Gent, Belgium

[⊥]EMAT, University of Antwerp, B-2020 Antwerp, Belgium

S *Supporting Information*

ABSTRACT: Pb cations in PbS quantum rods made from CdS quantum rods by successive complete cationic exchange reactions are partially re-exchanged for Cd cations. Using STEM-HAADF, we show that this leads to the formation of unique multiple dot-in-rod PbS/CdS heteronanostructures, with a photoluminescence quantum yield of 45−55%. We argue that the formation of multiple dot-in-rods is related to the initial polycrystallinity of the PbS quantum rods, where each PbS crystallite transforms in a separate PbS/CdS dot-in-dot. Effective mass modeling indicates that electronic coupling between the different PbS conduction band states is feasible for the multiple dot-in-rod geometries obtained, while the hole states remain largely uncoupled.

Colloidal quantum rods (QRs) are an attractive class of nanocrystals. Either grown out of a single material or as a heterostructure, the combination of quantum confinement and shape anisotropy results in materials with tunable, anisotropic opto-electronic properties. A typical example is heterogeneous CdSe/CdS dot-in-rods.[1,2] These materials exhibit a highly efficient, polarized photoluminescence (PL) tunable from green to red, and their homogeneity allows them to assemble them in close-packed ordered arrays.[3] However, with bulk bandgaps of 1.74 (CdSe) or 2.40 eV (CdS), cadmium chalcogenide (CdX) QRs are mainly of interest for applications involving visible light. In this Communication, we extend the PL wavelength range of colloidal QRs to the near-IR by demonstrating the formation of efficiently emitting heteronanorods that feature multiple PbS dots in a single CdS rod.

In the case of CdX, rod growth is made possible by the combination of an anisotropic crystal structure (wurtzite) and specific surface ligands (phosphonic acids).[4] The synthesis of QRs active in the near-IR (~800−3000 nm) has proved to be more challenging. Lead chalcogenides (PbX), the most widely used near-IR quantum dots (QDs), have a cubic crystal structure. In that case, rod or wire growth has only been achieved with indirect methods such as chelation of the precursors,[5] heterogeneous seeding,[6] cationic exchange,[7] or oriented attachment of QDs.[8] In the case of cationic exchange, it was shown that CdS QRs can be transformed into PbS QRs by two successive exchange steps. This has the advantage that the enormous variety of sizes, aspect ratios, and materials accessible via CdX QR synthesis can transferred to PbX QRs.

However, by repeating the procedure proposed by Luther et al.,[7] we found that an important drawback of the resulting PbS QRs is a low PL quantum yield (PLQY). This makes these materials, unlike CdSe/CdS dot-in-rods, not appropriate for high-end applications such as wavelength down-conversion or optical amplification.

Here, we show that near-IR QRs with high PLQY can be made by extending the cationic exchange approach with one additional step in which Pb is partially replaced by Cd. By controlling the exchange conditions, this results in PbS/CdS QRs with a PLQY of 45−55%. Moreover, high-angle annular dark-field scanning transmission electron microscopy (HAADF-STEM) makes clear that the resulting heterostructures are composed of a chain of multiple PbS dots embedded in a CdS rod. Although in this case electronic coupling between the different PbS dots appears to be small, the synthesis procedure provides extensive freedom for tuning. Hence, the approach presented here not only leads to anisotropic near-IR QRs with a high PLQY but also may enable the formation of electronically coupled QDs embedded in a single colloidal QR.

The starting materials are CdS QRs synthesized with a seeded growth approach following Carbone et al.[2] The successive Cd/Cu and Cu/Pb exchanges are promoted by methanol and tributylphosphine, respectively (see Supporting Information (SI)-S1).[7] Focusing on CdS rods with dimensions of (diameter:length) 3.7:28 nm (sample A, Figure 1a), we find that the successive exchange steps transform the absorption peak of the CdS bandgap transition at 480 nm to a shoulder at 1100 nm, which is characteristic of PbS (Figure 1b). Figure 1c shows that the PbS QRs thus formed are polycrystalline, with the different crystallites separated by [111] twin planes (see SI-S2 for more complete structural characterization). A similar observation was reported by Luther et al.,[7] who interpreted this as a result of the formation of two PbS segments at either end of the rod, resulting in a grain boundary where the reaction fronts meet. Here, high-resolution TEM indicates that the PbS QRs can be composed of more than two segments (Figure 1c). In the example given, five segments can be discerned, but their actual number changes depending on, e.g., the length of the QR. This indicates that the exchange can also start at the sides of the QRs. Possibly, this is driven by stacking faults in the original CdS rods (see SI-S2.2).
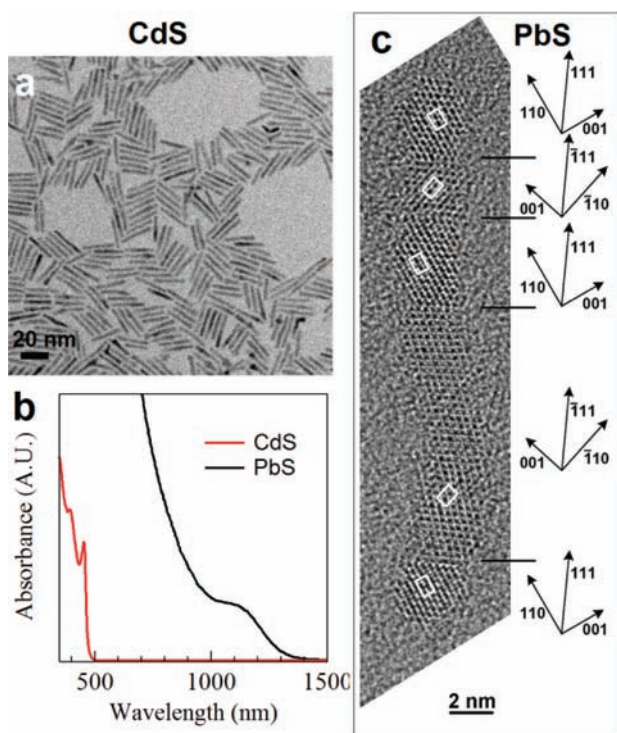
Figure 1. (a) Overview TEM image of starting CdS QRs. (b) Absorption spectra of CdS and PbS QRs from the same starting material. (c) HR-TEM image of a PbS QR on a [110] zone axis. The white rectangles indicate the ⟨110⟩ unit cell, and the arrows show the three major crystal directions in the five crystal segments that constitute the rod.

STEM-energy-dispersive X-ray (EDX) indicates that the rods made by successive cationic exchange contain only Pb and S. Nevertheless, STEM-HAADF imaging (see SI-S2.3) shows that small, 1−2 nm clusters are present at their surface. Since the STEM-HAADF signal intensity increases with the atomic weight of the element probed, these clusters are Pb rich as compared to the PbS QRs. Possibly, these are PbS clusters with a Pb surface termination or metallic Pb particles.

The main drawback of the resulting PbS QRs is their low PLQY of about 9%. In the case of PbX QDs, growth of a CdX shell by cationic exchange has been proposed as a way to enhance and stabilize the PLQY.[9,10] In line with this result, we have exposed a suspension of PbS QRs in toluene to an excess of Cd oleate at elevated temperature. Elemental analysis by TEM-EDX shows that this leads to a progressive replacement of Pb by Cd, which is more pronounced the longer the reaction time or the higher the temperature (Figure 2a). For exchange temperatures of 65−100 °C, 45−95% of the Pb atoms are replaced by Cd, corresponding to a nominal shell thickness of 0.4−1.2 nm, respectively. As compared to the original PbS QRs, the PL spectrum of the PbS/CdS heterorods shifts to shorter wavelengths, and, more importantly, the PLQY increases sharply. After 120 min of shell growth, it reaches 45 or 55% if the exchange is done at 65 or 80 °C, respectively.

The morphology of the QRs was studied in detail using STEM-HAADF. With core/shell PbS/CdS heterorods, this should result in images showing a bright (PbS) core and a darker (CdS) shell. This is not what is observed. For sample A, with the final Pb-for-Cd exchange done at 65 °C, the overview image (Figure 3a) already shows that each rod is composed of a series of brighter and darker segments, featuring 4−5 bright
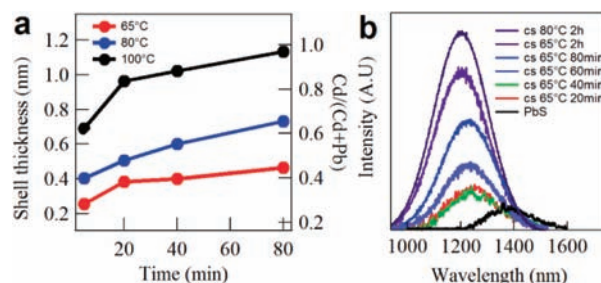

Figure 2. (a) Evolution of the ratio Cd/(Pb+Cd) and the nominal CdS shell thickness as a function of the reaction time for different reaction temperatures (sample A rods). (b) Evolution of the PL spectrum with reaction time for an exchange reaction at 65 °C, and final PL spectrum for an exchange reaction at 80 °C (sample A rods).
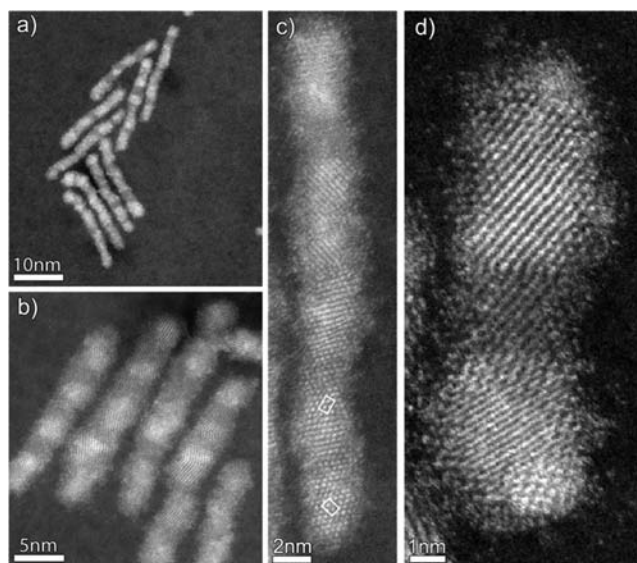

Figure 3. STEM-HAADF images of PbS/CdS rods showing multiple PbS QDs inside the rods recorded on (a−c) sample A and (d) sample B. The white rectangles in (c) indicate the ⟨110⟩ unit cell.

parts. Figure 3b demonstrates that the bright segments are embedded in the darker rod. We interpret this as evidence for the formation of multiple PbS dots in a single CdS rod. Similar results are obtained when starting from CdS rods with different aspect ratios (sample B, 4:14 nm; sample C, 5:16.5 nm, SI-2.4 and 2.5) and when starting from CdSe rods (sample D, SI-2.6). A high-resolution STEM image (Figure 3c) shows that the polycrystallinity of the original PbS QRs is maintained in the PbS/CdS heterorods. Especially in the case of sample B rods, STEM-HAADF indicates that each PbS crystallite is trans-formed into a single PbS/CdS segment (Figure 3d). This indicates that the multiple dot-in-rod heterostructures form because the cationic exchange proceeds quickly along the (defect-rich) interfaces between the original PbS segments. Importantly, this suggests that the morphology of these multiple dot-in-rod heterostructures can be tuned by adjusting the size of the PbS segments in the original PbS rods. Possibly, these reactive interfaces account for the difference with PbX rods made by oriented attachment, where partial Pb/Cd exchange rarely leads to multiple dot-in-rods.[11]

Averaging 150 embedded PbS dots (sample A), we find an effective average diameter of 3.7 nm, with a size dispersion of 15%. Similar results, albeit with less homogeneous PbS dots, are

obtained with a Pb-for-Cd exchange at 80 °C (see SI-S3). Spherical PbS QDs of the same size have their first exciton absorption and emission at 1100 and 1200 nm, respectively. For the multiple dot-in-rods, we obtain a shoulder in the absorption spectrum at 1050 nm and a PL maximum at 1200 nm. This correspondence suggests that electronic coupling between the PbS dots in a single PbS/CdS multiple dot-in-rod is limited. To analyze this further, we used effective mass modeling to calculate the electron and hole states (see SI-S4) in a hypothetical 3.7:28 nm CdS rod containing two PbS dots of radius R separated by a distance L_{sep}. Electronic coupling between conduction and valence band states is quantified by the energy splitting between the resulting bonding and antibonding states in this double-dot geometry (Figure 4b).
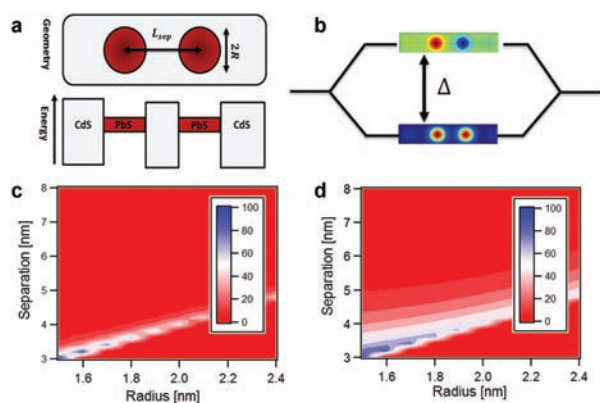

Figure 4. (a) Simulation geometry of (red) two PbS dots of radius R in a (grey) CdS rod separated by L_{sep}. (b) Energy diagram of the bonding and antibonding states obtained after electronic coupling of the two dots. (c,d) Energy difference between the bonding and antibonding states as a function of dot radius (x axis) and dot-dot separation (y axis) for (c) the higher energy hole state and (d) the lowest energy electron state. Only the region where $L_{sep} > 2R$ is physically relevant.

Similar to what was found with PbSe/CdSe, we find that the hole states remain confined in the PbS dots due to the large mismatch between the hole effective masses in PbS and CdS.[12] The probability to find the hole in a core PbS region is around 80%. As shown in Figure 4c, the concomitant hole coupling is negligible unless L_{sep} reaches the dot diameter $2R$. On the other hand, the smaller difference between the electron effective masses leads to leakage of the electron wave function outside the PbS dots (Figure 4d), resulting in a more significant coupling. Calculations show that the probability to find the electron in the CdS shell region is close to 40%. For $R = 1.85$ nm, an energy splitting comparable to $k_B T$ is achieved for a center-to-center distance less than 5 nm. This suggests that a 28 nm CdS rod containing 4−5 PbS dots is at the edge of the regime where quantum coupling between adjacent dots influences the optical properties of a multiple dot-in-rod PbS/CdS at room temperature.

In conclusion, we have used successive cationic exchange steps to synthesize colloidal PbS/CdS heterorods with a high PLQY in the near-IR out of CdS quantum rods. The successive, complete Cd/Cu and Cu/Pb exchanges lead to polycrystalline PbS QRs with a limited PLQY. A final Cd/Pb partial exchange raises the PLQY up to 55%. Instead of simple core/shell structures, this results in the formation of multiple dot-in-rod heterostructures, probably because each PbS segment in the original PbS QR is transformed into a single PbS/CdS unit. The number of PbS dots in a single rod depends on the original CdS rod length, and similar results are obtained when starting from CdSe rods. Since further tuning is possible by limiting the extent of the final cationic exchange,[7] this shows that successive cationic exchange is a versatile approach to form complex anisotropic heteronanostructures active in the IR. The correspondence between the first exciton absorption and emission wavelengths of the PbS/CdS multiple dot-in-rods and simple PbS dots suggests that quantum coupling between the dots in a single rod is limited for the geometries studied here, a conclusion supported by effective mass calculations. Nevertheless, the novel nanostructures developed here—providing unique colloidal QRs with high PLQY in the near-IR—can spark a wide range of follow-up research. This may involve pushing the system toward quantum coupling, extending the approach to other materials systems like PbSe/CdSe, a detailed analysis of the exciton fine structure, quantum coupling the properties of multiple excitons, and the development of applications in, e.g., solar concentrators and QD-based near-IR light sources.

ASSOCIATED CONTENT

Ⓢ Supporting Information

Synthesis and characterization of all the described systems and effective mass modeling of PbS/CdS multiple dots-in-rod. This material is available free of charge via the Internet at http://pubs.acs.org.

AUTHOR INFORMATION

Corresponding Author

Zeger.Hens@UGent.be

Notes

The authors declare no competing financial interest.

ACKNOWLEDGMENTS

REFERENCES

(1) Talapin, D. V.; Koeppe, R.; Götzinger, S.; Kornowski, A.; Lupton, J. M.; Rogach, A. L.; Benson, O.; Feldmann, J.; Weller, H. *Nano Lett.* **2003**, *3*, 1677.

(2) Carbone, L.; Nobile, C.; De Giorgi, M.; Sala, F. D.; Morelle, G.; Pompa, P.; Hytch, M.; Snoeck, E.; Fiore, A.; Franchini, I. R.; Nadasan, M.; Silvestre, A. F.; Chiodo, L.; Kudera, S.; Cingolani, R.; Krahne, R.; Manna, L. *Nano Lett.* **2007**, *7*, 2942.

(3) Zanella, M.; Gomes, R.; Povia, M.; Giannini, C.; Zhang, Y.; Riskin, A.; Va nBael, M.; Hens, Z.; Manna, L. *Adv. Mater.* **2011**, *23*, 2205.

(4) Peng, X. G.; Manna, L.; Yang, W. D.; Wickham, J.; Scher, E.; Kadavanich, A.; Alivisatos, A. P. *Nature* **2000**, *404*, 59.

(5) Lifshitz, E.; Bashouti, M.; Kloper, V.; Kigel, A.; Eisen, M. S.; Berger, S. *Nano Lett.* **2003**, *3*, 857.

(6) Yong, K.-T.; Sahoo, Y.; Choudhury, K. R.; Swihart, M. T.; Minter, J. R.; Prasad, P. N. *Nano Lett.* **2006**, *6*, 709.

(7) Luther, J. M.; Zheng, H. M.; Sadtler, B.; Alivisatos, A. P. *J. Am. Chem. Soc.* **2009**, *131*, 16851.

(8) Koh, W.-k.; Bartnik, A. C.; Wise, F. W.; Murray, C. B. *J. Am. Chem. Soc.* **2010**, *132*, 3909.

(9) Pietryga, J. M.; Werder, D. J.; Williams, D. J.; Casson, J. L.; Schaller, R. D.; Klimov, V. I.; Hollingsworth, J. A. *J. Am. Chem. Soc.* **2008**, *130*, 4879.

(10) Lambert, K.; De Geyter, B. D.; Moreels, I.; Hens, Z. *Chem. Mater.* **2009**, *21*, 778.

(11) Casavola, M; van Huis, M. A.; Bals, S.; Lambert, K.; Hens, Z.; Vanmaekelbergh, D. *Chem. Mater.* **2012**, *24*, 294.

(12) De Geyter, B.; Justo, Y.; Moreels, I.; Lambert, K.; Smet, P. F.; Van Thourhout, D.; Houtepen, A. J.; Grodzinska, D.; de Mello Donega, C.; Meijerink, A.; Vanmaekelbergh, D.; Hens, Z. *ACS Nano* **2011**, *5*, 58.